Progress In Electromagnetics Research C, Vol. 121, 1–18, 2022

A Circularly Polarized Quad-Band Wearable Textile Antenna Integrated with Triple Band AMC Reflector for WBAN Applications

Anil Badisa[1], Boddapati T. P. Madhav[1, *], Kantamaneni Srilatha[1], Myla C. Rao[2], and Sudipta Das[3]

Abstract—A quad-band (3.5, 5.8, 7.5 & 8.08 GHz), low profile, low Specific Absorption rate (SAR), and circularly polarized (3.5, 7.5, 8.08 GHz) wearable textile antenna ($50 \times 30 \times 1\,\text{mm}^3$) integrated with a triple-band zero reflection phase Artificial Magnetic Conductor (AMC) surface is presented. The designed standalone antenna exhibits low SAR with 10 mm separation for 0.5 W input power and radiation performance with a gain of > 5 dB and Front to Back Ratio (FBR) (< 10 dB) at all operating frequencies. The AMC unit-cell is synthesized using PDMS (Polydimethylsiloxane) with the footprint of $20 \times 20 \times 1\,\text{mm}^3$ to operating at 3.5, 7.5, and 8.08 GHz, respectively, with in-phase reflection. The designed 3×3 AMC reflector is integrated to improve the radiation performance of the designed antenna with gain to > 7 dB, FBR to > 10 dB, and withstanding low SAR at increased input power compatibility at separation ($d = 3$ mm) from the body surface. The designed AMC transforms the radiation pattern from omnidirectional to directional with improved FBR and reduced back radiation with low SAR (< 0.504 W/kg). The proposed AMC integrated antenna also providing mechanical feasibility in terms of handling the frequency detuning due to bending and the human-body loading feature makes it suitable for wireless body area networks (WBAN) applications.

1. INTRODUCTION

The demand, applications, and requirements of wearable devices in WBAN have been extensively increasing across all aspects of human life, e.g., health care, security data processing, and entertainment, as shown in Figure 1. In this process, wearable antenna plays an important role that is responsible for wireless links concerning body-centric communication in WBAN [1]. As a significant element, the design of a wearable antenna has to satisfy the requirements like low profile, safety, CP (Circular Polarization), light weight, radiation performance coupled with the human body, multi-bands, multi-functionalities, and easy integration, which is different from conventional antenna design aspects. The simultaneous agreement of all these requirements is a very challenging task in wearable antenna design [2].

As wearable antennas are operating very near the human body, the loading effects on antenna performance like frequency detuning and radiation performance effects have to be addressed while the model is designed. The effect on the human body due to the antenna placement in terms of SAR has to be as minimum as possible with the support of high-power handling capacity, which is also much desirable for today's wearable applications. Along with them, a good radiation performance like high gain and high FBR with reduced back radiation is also required for wearable antennas [3]. Wearable antenna must provide stable operation with various bending conditions concerning the human body dynamics while the biomechanical aspects like flexibility, low profile, light weight and biodegradability also have

Received 25 February 2022, Accepted 23 May 2022, Scheduled 14 June 2022

* Corresponding author: Boddapati Taraka Phaneendra Madhav (btpmadhav@kluniversity.in).

[1] Antennas and Liquid Crystals Research Center, Department of ECE, Koneru Lakshmaiah Education Foundation, AP, India. [2] Department of Physics, Andhra Loyola College, Vijayawada, AP, India. [3] Department of ECE, IMPS College of Engineering, West Bengal, India.

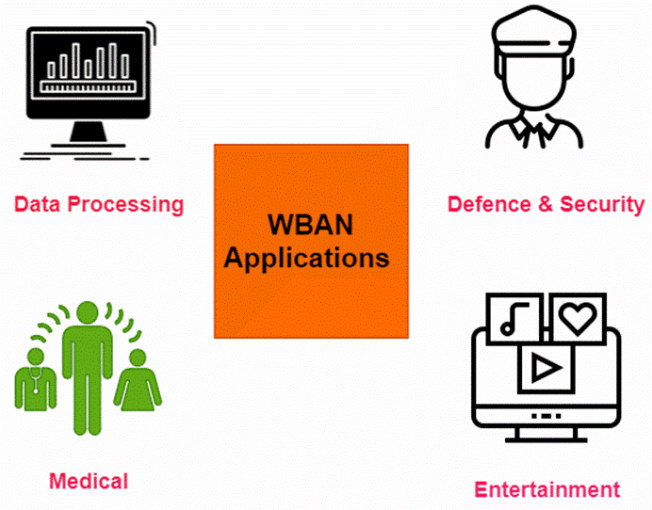

Figure 1. WBAN applications.

to be satisfied. For flexibility, various substrate materials like textiles, polymers, paper substrates have been utilized for wearable antenna designs [4].

The application of metamaterial concepts to wearable antennas is improving and demonstrated in [5–7]. AMC is a meta-surface that acts as a reflector with a reflection bandwidth of $\pm 90^{\circ}$ by providing a zero-reflection phase that provides constructive interference. Due to this mechanism, the radiation performance of the antenna-like gain, FBR is improved with reduced SAR [8]. Besides, the AMC surface provides isolation when being coupled with the human body by reducing frequency detuning [9, 10].

Various types of antennas reported in [11–14] operate with single band of operation only. Dual band operations with flexible and conformal substrates like textile and polymers with compact size are reported in [15–17] with low profile, high gain, circular polarization [18], and bidirectional radiation fields [19]. Various EBG structures are utilized in [20–22] for radiation enhancement but lack in directional radiation patterns. Moreover, wearable antennas need high FBR to reduce back radiation towards human body surface using DGS structures [23, 24] and converting the cross polarized fields [25, 26]. Various AMC structures were proposed in the literature [27–32] for wavefront manipulation that is not concerning all the wearable antenna requirements like multiband, circularly polarization, low profile, and low SAR. Hence, the designed antenna performance is investigated for these requirements and challenges, and the significant results are obtained with AMC integration.

In this paper, a circularly polarized wearable quad-band textile antenna integrated with triple-band AMC is proposed which satisfies the requirements of wearable antennas. The Jeans based embroidered antenna resonates at Wi-Max (3.5 GHz), ISM (Industrial Scientific Medical Bands) (5.8 GHz), Mobile communication (7.5 GHz), and satellite communication (8.08 GHz) applications with triple-band circular polarization. The design and analysis of the textile antenna are presented in Section 2. In Section 3, a PDMS-based unit cell with dimensions of $20 \times 20 \times 1\,\text{mm}^3$ is designed with triple zero reflection phases at 3.5 GHz, 7.5 GHz, and 8.08 GHz, respectively, which acts as a reflector. The periodic array of unit-cell, i.e., 3×3 AMC surface is proposed and analyzed with the focus on radiation performance in the improvement of gain and FBR with low SAR. The SAR is analyzed for the flexible AMC integrated antenna with variable distance (d) from the human body surface and input power variation. The results show that the suggested antenna is able to handle high input power, reduced frequency detuning, and small separation distance with low SAR values. Using the proposed AMC reflector, the enhanced radiation performance in terms of gain by 1.76, 1.4, 0.76, 0.22 dB, and FBR by 9.78, 6.88, 2.04, 8.41 dB at 3.5 GHz, 5.8 GHz, 7.5 GHz, and 8.08 GHz, respectively. The design and analysis of the proposed antenna have been done in the CST Microwave studio full-wave simulation tool. The fabricated prototype is characterized using Anritsu Vector Network Analyzer (MS2037C). The consistency in measured results shows the suitability of the proposed antenna for WBAN applications.

2. DESIGN & ANALYSIS OF QUAD-BAND TEXTILE ANTENNA WITH CP

2.1. Quad-Band Textile Antenna Design

The antenna layout of the proposed circularly polarized quad-band textile antenna is shown in Figure 2. The antenna is designed using a jeans substrate ($\varepsilon_r = 1.7$, loss tangent 0.025) with dimension $50 \times 30 \times 1\,\text{mm}^3$. Horizontal and vertical stubs are arranged with L slots that make the antenna operate at quad bands (3.5, 5.8, 7.5, 8.08 GHz) with triple-band circular polarization (CP). The concept of current path distribution through $\lambda_g/4$ length stubs (λ_g = guided wavelength) is considered as a design method. To fabricate the antenna, an embroidered conductive thread with properties of resistivity ($< 1\,\text{k}\Omega/10\,\text{cm}$), 180-micron diameter from Less EMF [33] is used. The simulated and measured reflection coefficients (dB) are shown in Figure 3.

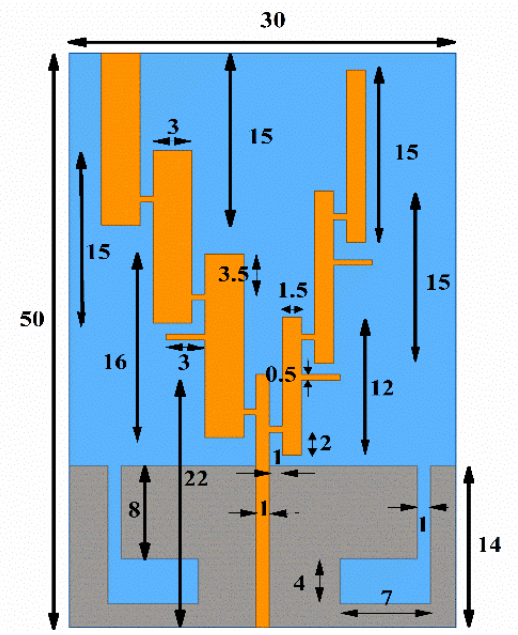

Figure 2. Reference antenna structure (dimensions in mm).

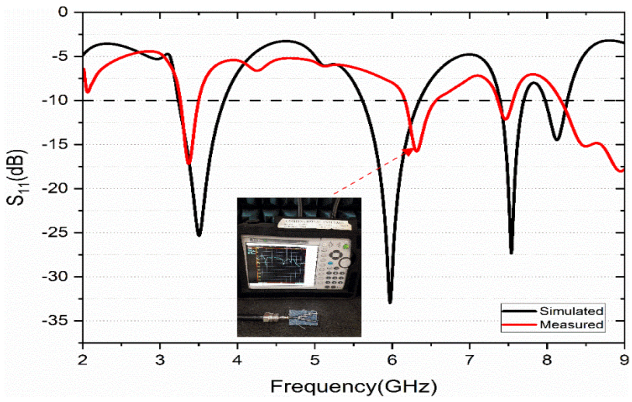

Figure 3. Standalone antenna reflection coefficient.

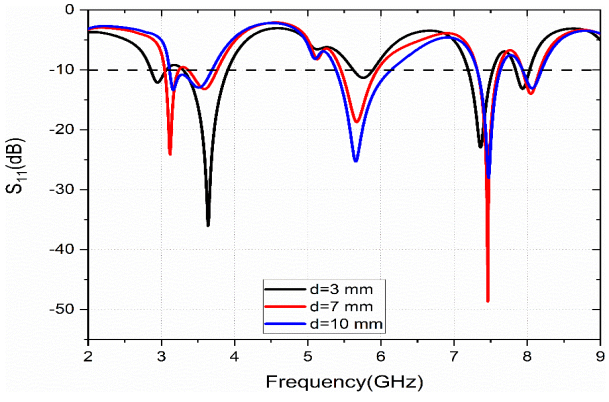

Figure 4. Reflection coefficient vs frequency with variable distance (d) from the human-body surface.

2.2. Antenna Performance Analysis

The antenna performance summary of far-field parameters is presented in Table 1. The quad-band antenna performs well with good gain, efficiency, and circular polarization in free space. But in wearable cases, the antenna has to be loaded with the human body, thereby the effect has to be minimized to provide stable operation. The effect of human body loading with proximity is presented in terms of frequency detuning in reflection coefficient, shown in Figure 4. It is observed that with the closing value of d (mm), more effect of detuning occurs which is not suitable for low-profile wearable antennas. The human body effect is studied using the setup presented in Figure 5.

Table 1. Standalone antenna radiation performance.

Frequency-(GHz)	**Gain-(dB)**	**FBR-(dB)**	**Efficiency-(dB)/%**
3.5	5.77	0.935	−2.22/60
5.8	7.68	4.92	−1.94/64
7.5	7.42	12.46	−1.19/76
8.08	7.43	7.75	−1.80/66

The effect on the human body surface due to antenna radiation is analyzed for SAR value. The standard reference of SAR value is 1.6 W/kg, 2 W/kg for 1 g, 10 g of human body tissue respectively standardized by FCC (Federal Communications Commission) [34]. The reference antenna is studied with human body proximity (d mm) analysis for SAR (W/Kg) that is presented in Table 2. Satisfying results are observed for $d = 10$ mm separation between the antenna and human body surface. The SAR distribution of the antenna at 3.5 GHz operating frequency is presented in Figure 5. The properties of phantom model for simulation are shown in Section 3.3.

Table 2. SAR proximity analysis with variable d (mm).

Frequency (GHz)	$d = 3$		$d = 7$		$d = 10$	
	1 g.	**10 g.**	**1 g.**	**10 g.**	**1 g.**	**10 g.**
3.5	24.1	8.61	14.4	5.36	0.475	0.384
5.8	13.1	3.15	4.8	2.15	0.392	0.22
7.5	6.75	1.88	3.01	1.08	0.534	0.255
8.08	5.71	1.78	2.01	0.79	0.402	0.212

These effects of frequency detuning and proximity have to be minimized for the wearable antenna. Further, the gain and FBR have to be improved. The designed AMC surface provides all these requirements that act as a reflector with improved gain and FBR, by controlling radiation pattern which in turn provides good isolation characteristics between the antenna and the human body. The design and analysis of AMC reflector integration with antenna are presented in the following section.

3. DESIGN & ANALYSIS OF AMC REFLECTOR INTEGRATED ANTENNA

In this section, the design methodology of the proposed unit cell that is resonating at triple bands (3.5, 5. 8 and 8.08 GHz) with 0°-reflection phase is presented. The main function of the AMC reflector is to improve gain and FBR by controlling the wavefront. Another attribute of the proposed AMC integrated antenna is to isolate the antenna from human body loading closeness. The variable AMC array integration with the antenna is studied along with its radiation performance and human body proximity analysis of SAR. The comparative analysis of standalone antenna and AMC integrated antenna is also studied, and radiation performance improvement is observed by AMC integrated antenna.

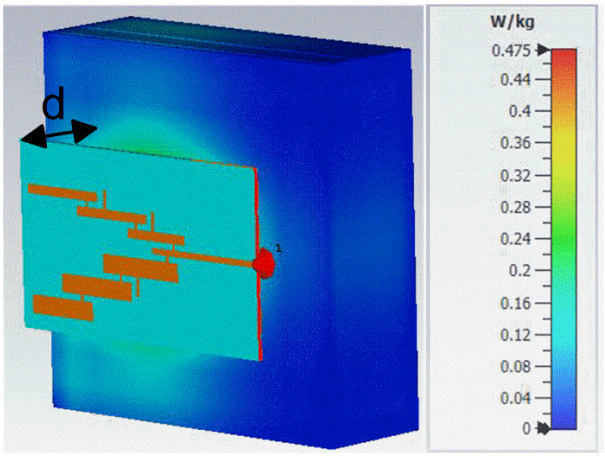

Figure 5. SAR value at 3.5 GHz with $d = 10$ mm (1 g of tissue).

3.1. Unit-Cell Design

The AMC unit-cell is designed using a PDMS substrate ($\varepsilon_r = 2.66$, $\tan\delta = 0.023$) [35] with dimensions of $20 \times 20 \times 1\,\text{mm}^3$. The iterative steps in the evolution process are shown in Figure 6, where rectangular ring slots are added to a basic square shape with full ground. The final Layout of the proposed unit cell with dimensions is represented in Figure 7(a) and Table 3.

$$\text{Resonating frequency}\,(f_r) = \frac{1}{2\pi\sqrt{\text{LC}}} \tag{1}$$

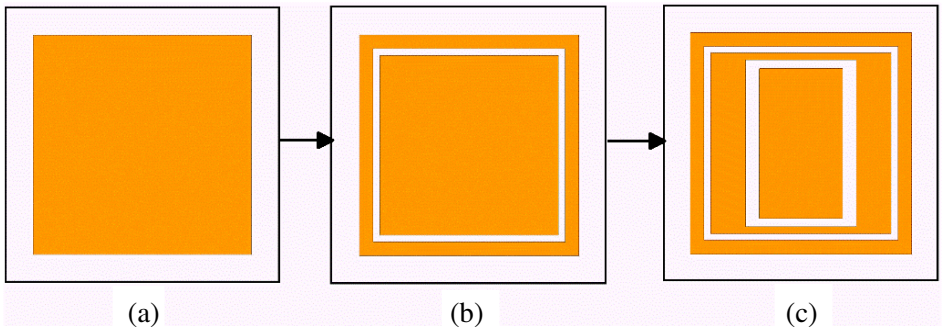

Figure 6. Unit cell design steps, (a) step 1, (b) step 2, (c) step 3.

Figure 7(b) represents the equivalent LC-circuit model for the given structure. These circuit parameters are calculated using Equation (1), where Z_{in} is the input impedance, and Z_{out} is the free space characteristic impedance [36].

The characteristics of the AMC cell with design steps in terms of reflection coefficient (dB) and reflection phase (degree) are shown in Figures 8(a) and (b). In each step, one resonating frequency is added with a corresponding 0°-reflection phase.

The unit cell parameters are optimized to make it resonate at 3.5 GHz, 5.8 GHz, 8.08 GHz frequencies with zero-reflection phase which acts as AMC reflector. The variation of slot parameters on the reflection coefficient is shown in Figures 9(a) and (b). The designed unit cell is integrated with the antenna as an AMC reflector array, and the radiation parameters improvement is analyzed in the following section.

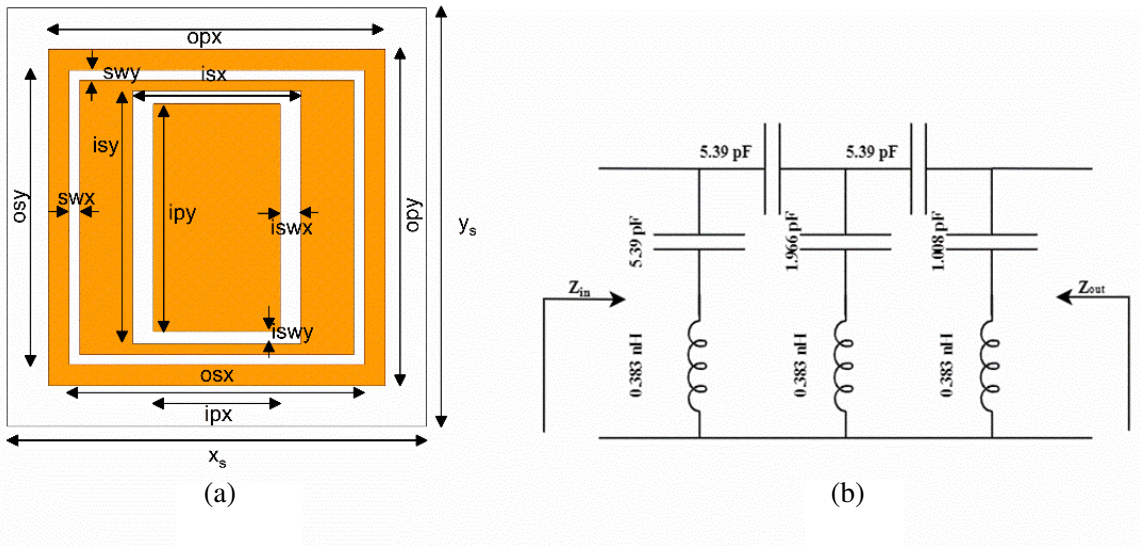

Figure 7. (a) Unit cell final layout. (b) LC-equivalent circuit model.

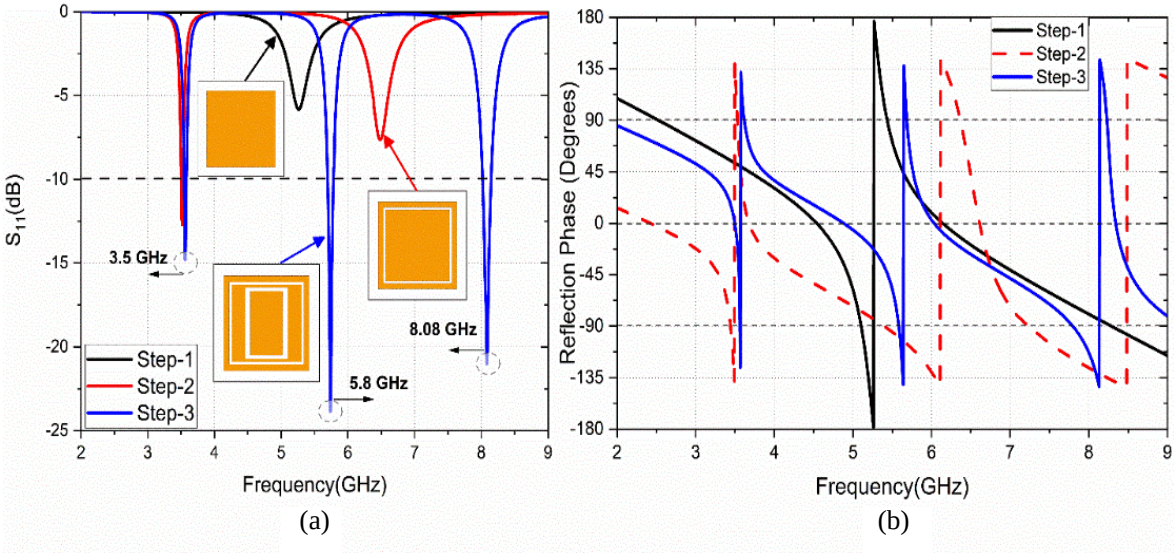

Figure 8. Unit cell characteristics. (a) S_{11} (dB) vs frequency. (b) Reflection phase (deg) vs frequency.

Table 3. Unit cell design parameters.

Variable	Value (mm)	Variable	Value (mm)
xs	20	ys	20
$iswy$	0.6	$iswx$	0.6
Isx	8	swy	0.5
osy	14	osx	14
opx	16	Ipy	10.8
ipx	6	swx	0.5
zs	1	opy	16
isy	12		

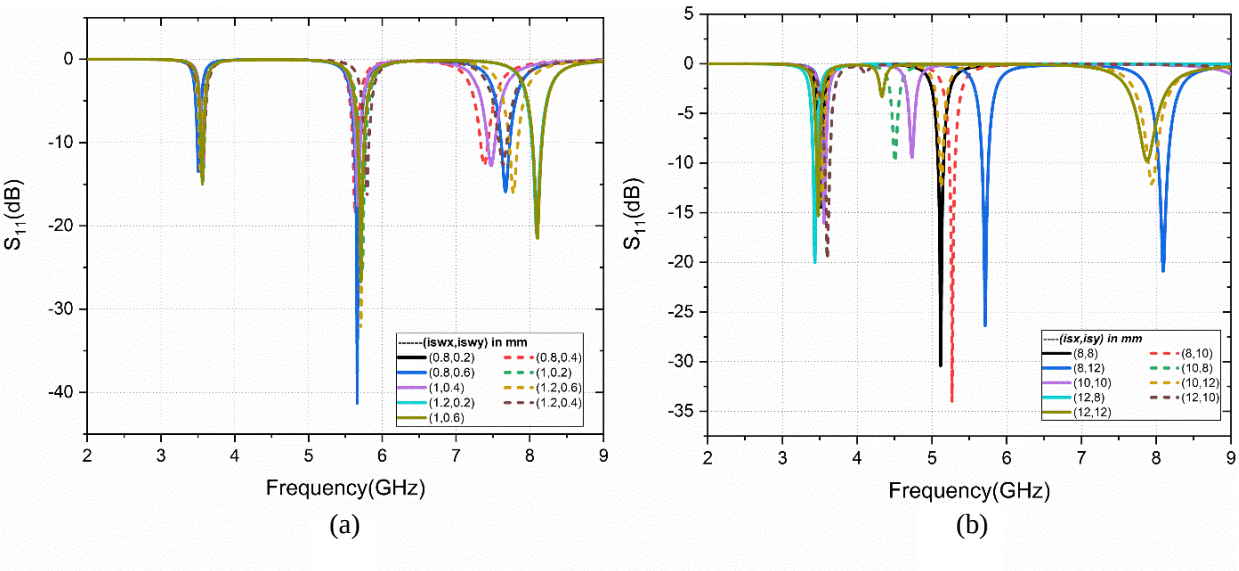

Figure 9. S_{11} (dB) vs frequency plot for slot parametric variation (mm). (a) $iswx, iswy$, (b) isx, isy.

3.2. Free Space Analysis of AMC Integrated Antenna

The Integration of the AMC reflector with the designed antenna set up along with its cross-sectional view is shown in Figure 10. The distance of separation is represented with variable h (mm).

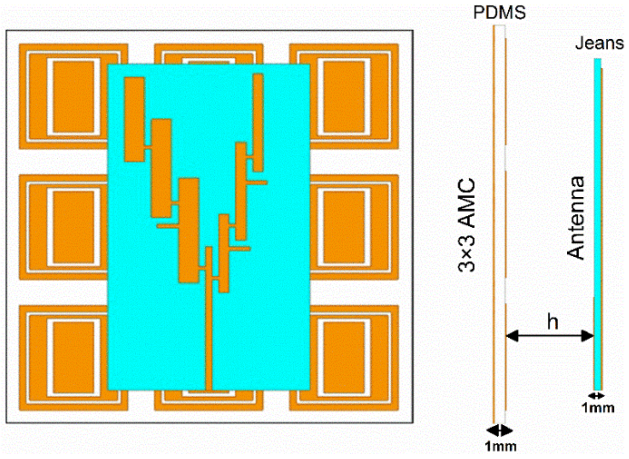

Figure 10. Proposed AMC integrated antenna with a cross-sectional view.

3.2.1. Analysis of Reflection Coefficient

The simulated results of the reflection coefficient with variable h in mm are presented in Figure 11. At $h = 15$ mm, the optimum results are obtained and considered for further analysis. The study and analysis of AMC array size are presented in Figure 12 with the combinations of 3×3, 4×3, 4×4 AMC arrays. The 3×3 AMC is selected due to appropriate operation with a low profile. The comparison between the reflection coefficients of the standalone antenna and AMC integration is shown in Figure 13.

The role of AMC instead of the full ground reflector is also presented in Figure 14 to illustrate the concept of constructive, destructive interference generated by AMC and full ground plane, respectively, due to which the peak value of the reflection coefficient is reduced in the case of a full ground reflector.

The AMC integrated antenna is analyzed for XY, YZ bending cases as shown in Figure 15. The

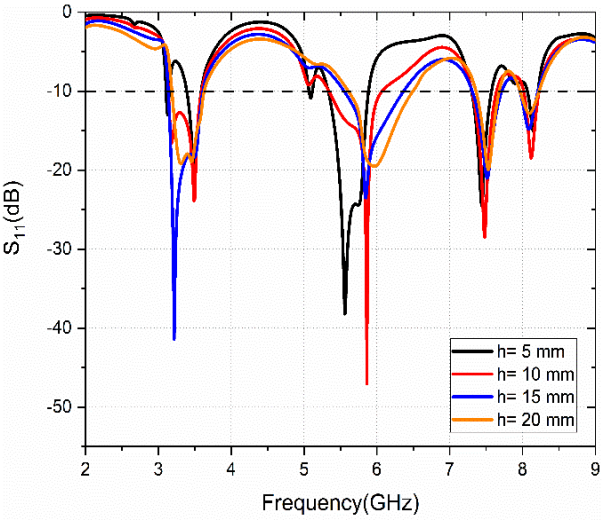

Figure 11. S_{11} (dB) vs frequency with h variation.

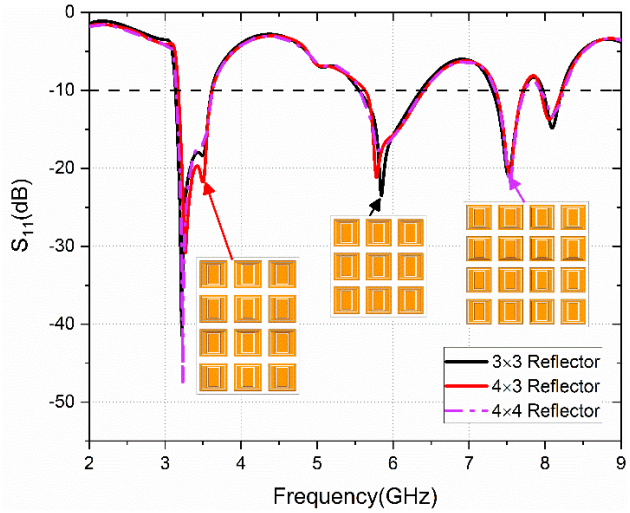

Figure 12. Reflection coefficient for AMC array sizes.

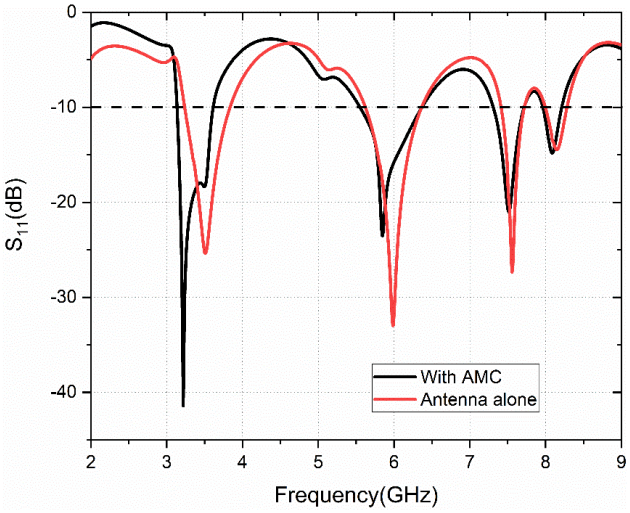

Figure 13. S_{11} (dB) vs frequency comparison.

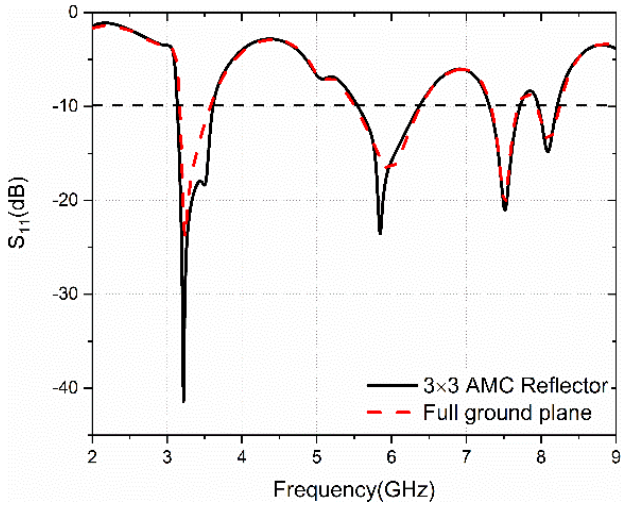

Figure 14. S_{11} (dB) for AMC and full ground reflector.

simulated reflection coefficient graphs under different conditions with angles 30°, 60°, and 90° are illustrated in Figures 16(a) and (b).

In the XY-bending case, with an increase in bending angle, the peak of the reflection coefficient is slightly affected. Compared to XY bending, the bending effect is more in YZ bending due to high variation in the effective length of the antenna.

3.2.2. Analysis of Radiation Performance

The designed antenna is operating with triple-band circular polarization. Figure 17 illustrates the axial ratio (dB) for frequency variation, in which for 3.5, 7.5, 8.08 resonant frequencies the axial ratio is < 3 dB. The proposed antenna provides similar surface current directions to the AMC backed antenna surface current distributions as presented in Figure 18. The current directions are indicated on the antenna structure that gives understanding of CP mechanism with orthogonal vector rotation in clockwise/anticlockwise. At 3.5 GHz, clockwise rotation and anticlockwise rotation are observed for

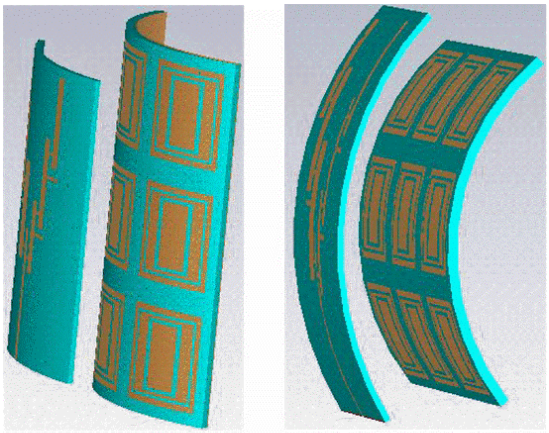

Figure 15. Bending configurations at 60°, (a) XY-bend, (b) YZ-bend.

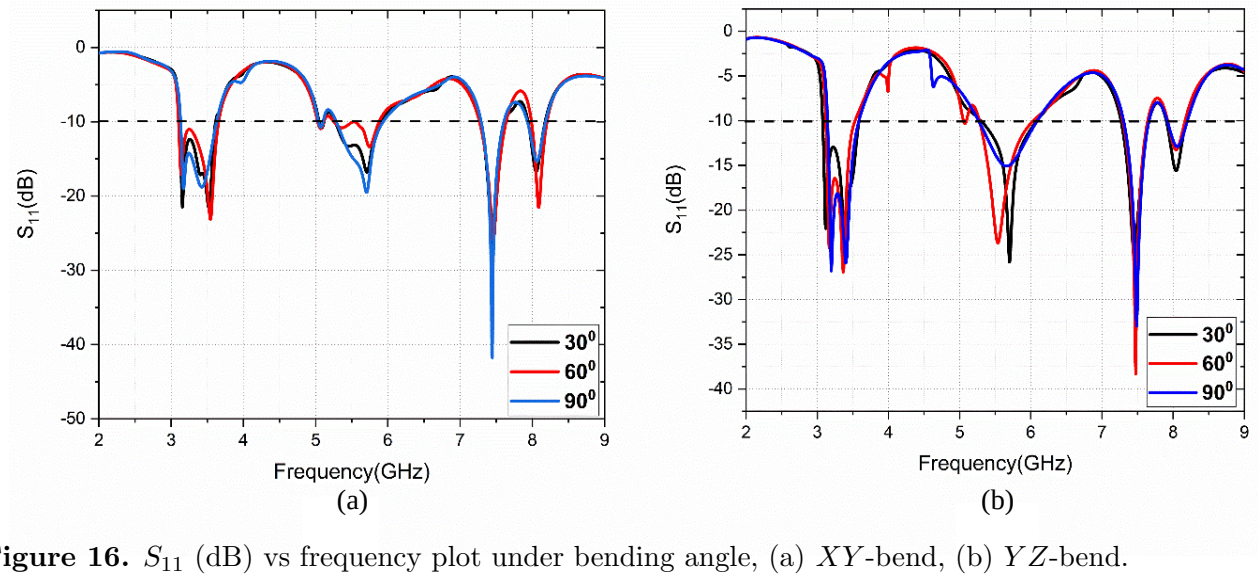

Figure 16. S_{11} (dB) vs frequency plot under bending angle, (a) XY-bend, (b) YZ-bend.

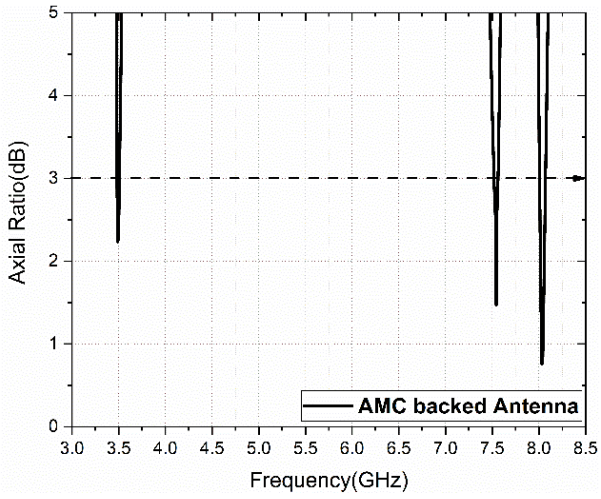

Figure 17. Simulated axial ratio plot.

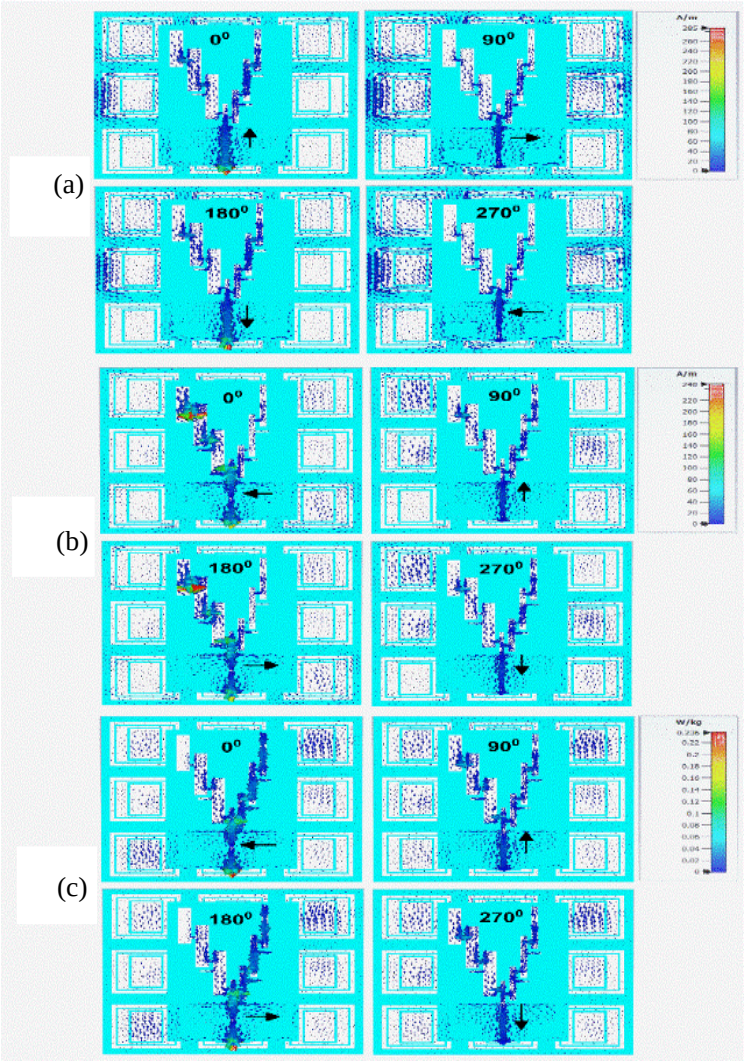

Figure 18. Simulated surface current distribution of AMC integrated antenna at f (GHz), (a) 3.5, (b) 7.5, (c) 8.08.

7.5 and 8.08 GHz frequencies.

The far-field characterization of the proposed AMC integrated antenna is analyzed using the setup shown in Figure 19. On the left side, the fabricated image of the proposed antenna is shown along with the microscopic image of the Embroidery patch radiator with 200X resolution.

The fabricated prototype is used for measured results with phi = 0°, 90° variations. The radiation patterns of the antenna and AMC integrated are represented as shown in Figure 20 for comparison, which depicts the wavefront controllability of the AMC reflector with in-phase reflection.

The 3D radiation patterns of the stand-alone antenna and AMC integrated antenna at 3.5 GHz are shown in Figure 21. The figure shows that the AMC reflector converts the omnidirectional radiation pattern into a directional radiation pattern, which increases the gain and FBR value.

Due to constructive interference, the FBR is improved to a value > 10 dB at all resonant frequencies, as shown in Figure 22. The quantity of efficiency improvement in comparison with an antenna alone is plotted in Figure 23.

The improved Gain (dBi) of the AMC array size integration is summarized in Table 4. The proposed 3×3 AMC array provides appropriate results at all operating frequencies.

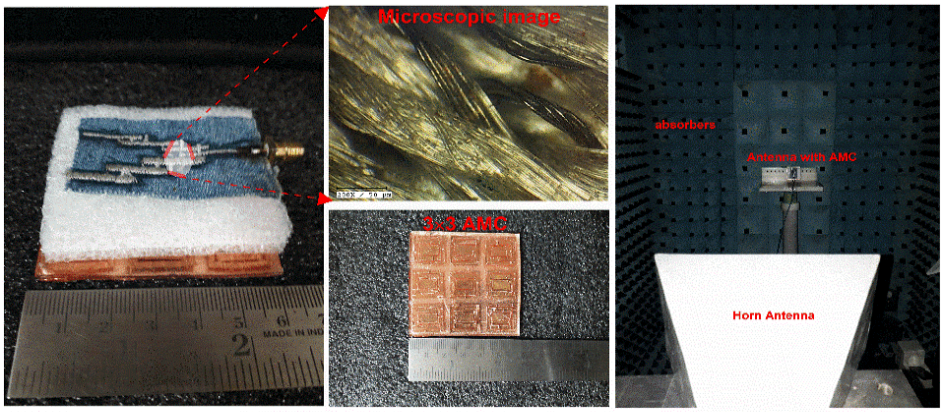

Figure 19. Experimentation setup. (a) Fabricated prototype with microscopic image. (b) Far-field measurement setup.

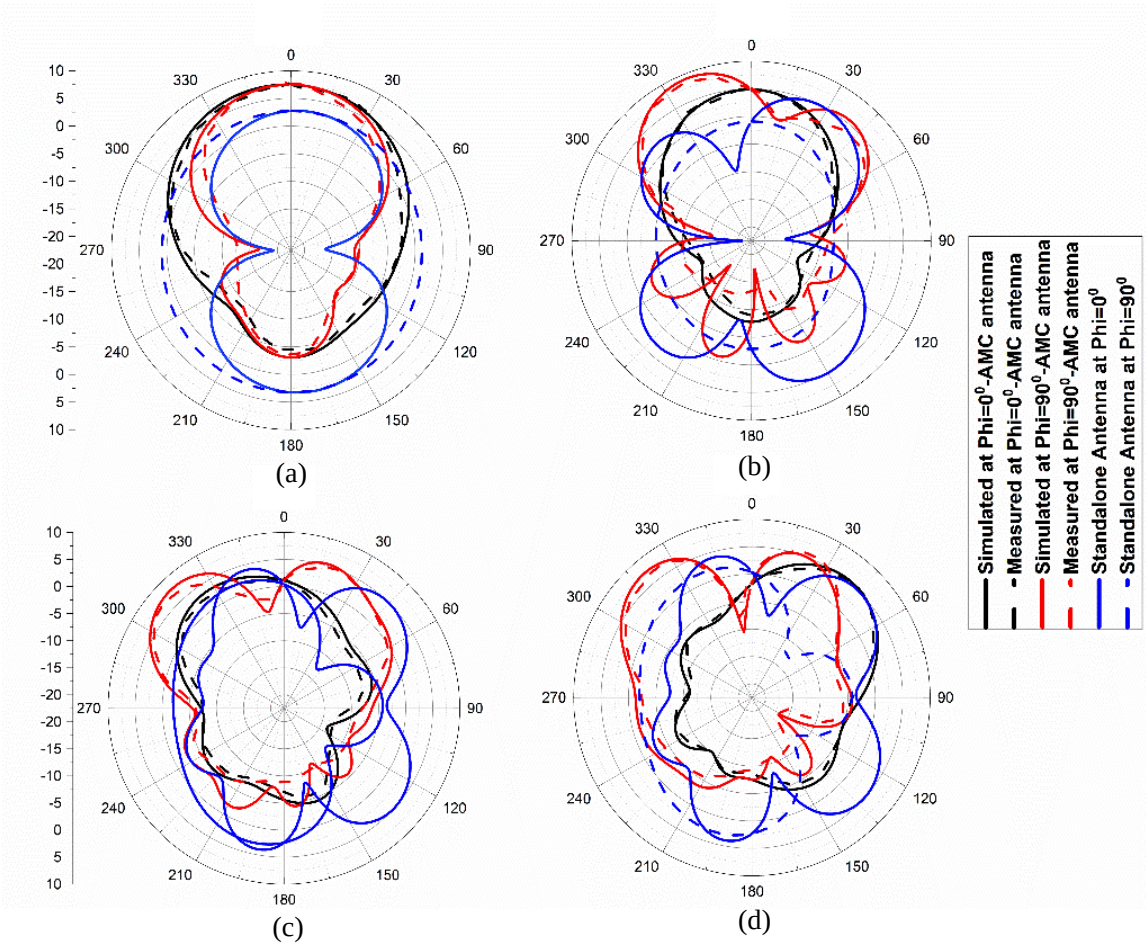

Figure 20. Comparison between radiation patterns of standalone antenna and AMC antenna, (a) 3.5, (b) 5.8, (c) 7.5, (d) 8.08 GHz.

3.3. Human Body Proximity Analysis

The human body loading effect reduction is one of the main challenges in wearable antenna design. So, the human body loading performance has to be investigated. Figure 24 represents the human body

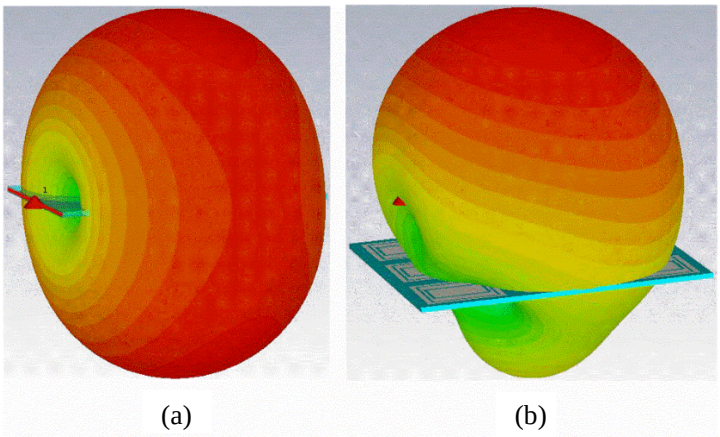

Figure 21. 3D gain plots comparison for 3.5 GHz at Phi = 0°. (a) Antenna alone. (b) Antenna with AMC.

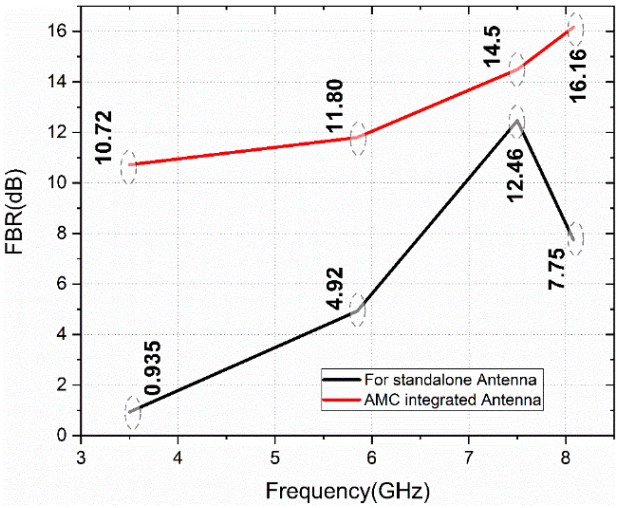

Figure 22. FBR comparison plot.

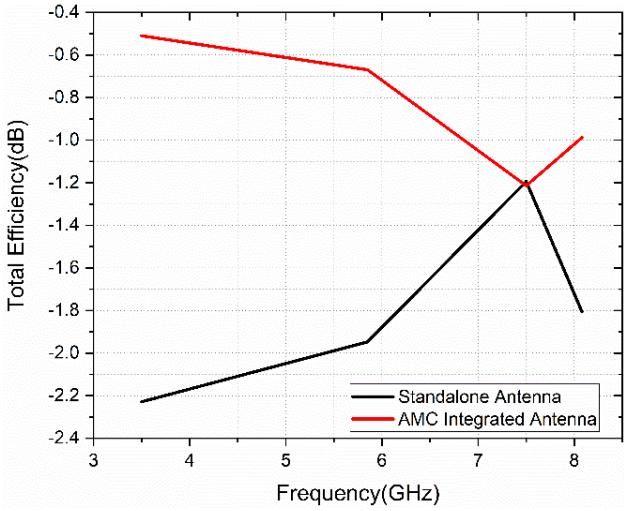

Figure 23. Efficiency comparison.

Table 4. Simulated gain comparison for variable AMC array size with standalone antenna.

Frequency (GHz)	Gain in dBi			
	Antenna Alone	3 × 3 AMC	4 × 3 AMC	4 × 4 AMC
3.5	5.77	7.53	7.21	5.61
5.8	7.68	9.08	9.57	6.15
7.5	7.42	8.18	9.05	9.63
8.08	7.43	7.65	8.32	9.41

phantom setup integrated with the AMC-backed antenna with proximity distance d (mm) in planar and curvature form. The properties of the Phantom, which are considered for SAR analysis, are shown in Table 5.

The comparative reflection coefficient (dB) plot for human body loading results is plotted in Figure 25. The AMC integrated antenna provides high isolation with human body proximity in contrast with the antenna. The reduction in S_{11} (dB) and frequency detuning in the standalone antenna body

Table 5. Simulated human body phantom model properties [26].

Tissue	Permittivity-(ε_r)	Conductivity-(S/m)	Density-(kg/m^3)	Thickness-(mm)
fat	5.173	0.155	930	6
muscle	51.44	2.557	1050	12
skin	35.11	3.717	1090	2

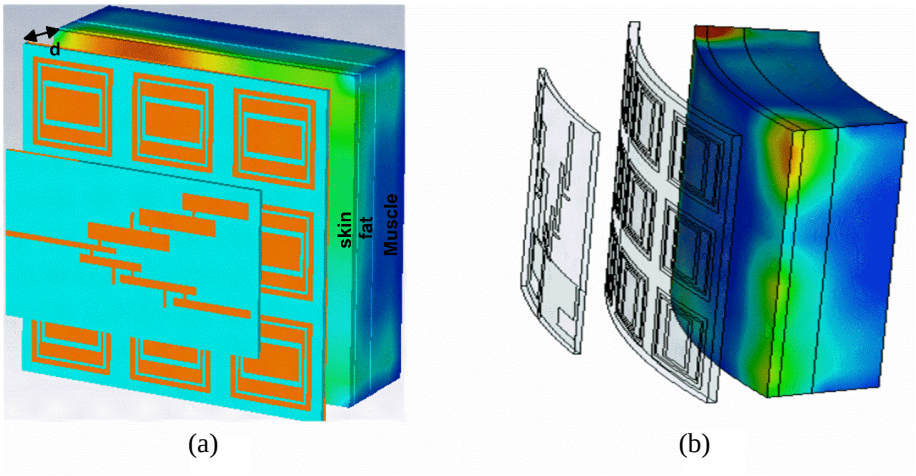

Figure 24. Human body model loaded antenna simulation setup. (a) Planar form, (b) bending at 90°.

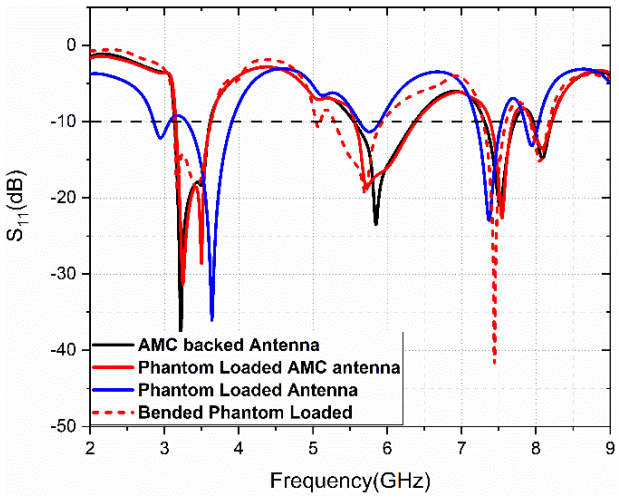

Figure 25. S_{11} (dB) with human body loading.

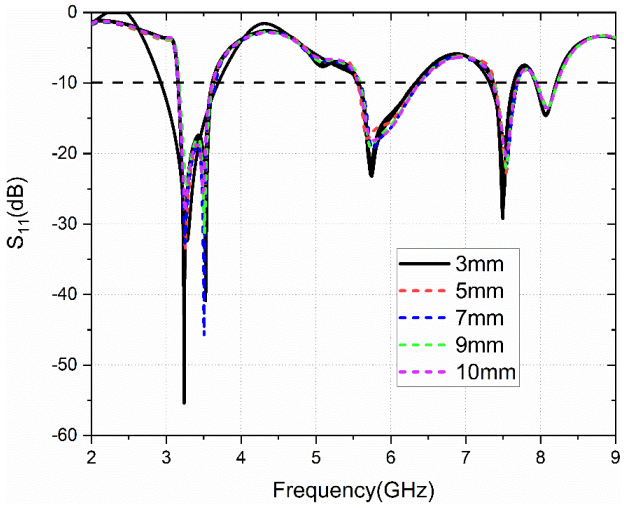

Figure 26. S_{11} (dB) with variable d (mm).

loading is compensated in addition to improvement in gain and FBR by providing good isolation.

The separation between the body surface and antenna is another consideration for the performance analysis of a wearable antenna. The antenna should avoid the frequency detuning in operating frequencies with high proximity. The proximity analysis with $d = 3$ mm is shown in Figure 26, which implies that the proposed antenna holds the isolation near the body surface.

Table 6. SAR variation with input power variation (P_{in}) at $d = 3\,\text{mm}$, $5\,\text{mm}$.

Frequency (GHz)	$P_{in} = 0.5\,\text{W}$ ($d = 3\,\text{mm}$)		$P_{in} = 1\,\text{W}$ ($d = 3\,\text{mm}$)		$P_{in} = 0.5\,\text{W}$ ($d = 5\,\text{mm}$)		$P_{in} = 1\,\text{W}$ ($d = 5\,\text{mm}$)	
	1 g	10 g	1 g	10 g	1 g	10 g	1 g	10 g
3.5	0.363	0.154	0.683	0.288	0.815	1.211	1.62	0.621
5.8	0.506	0.21	1.016	0.414	0.528	0.21	2.38	0.784
7.5	0.423	0.183	0.823	0.393	0.311	0.33	1.73	0.667
8.08	0.297	0.166	0.575	0.323	0.87	0.39	1.05	0.438

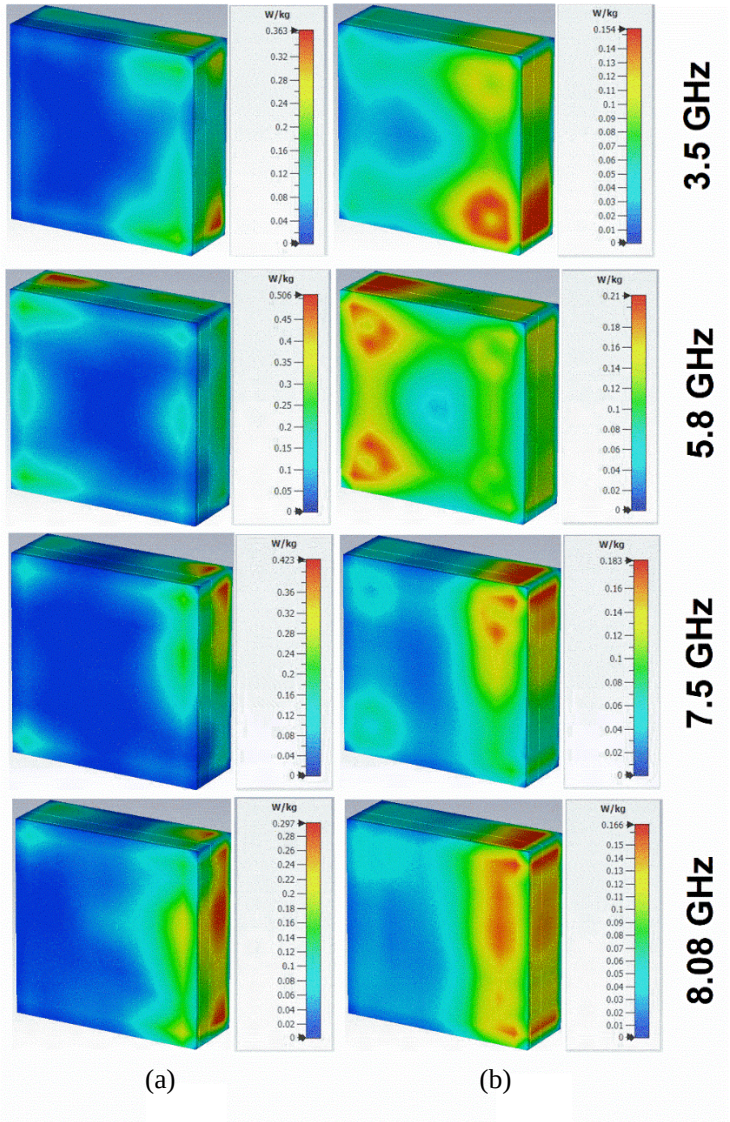

Figure 27. Simulated SAR distributions of AMC integrated antenna with $d = 3\,\text{mm}$ for resonate frequencies ($P_{in} = 0.5\,\text{W}$), (a) 1 g, (b) 10 g.

Table 7. Summary of AMC integrated antenna performance.

Frequency (GHz)	**Antenna alone**		**Antenna with 3×3 AMC**		**Human body Loading at $d = 3$ mm Gain (dBi)**
	Gain (dBi)	**FBR (dB)**	**Gain (dBi)**	**FBR (dB)**	
3.5	5.77	0.935	7.53	10.72	8.08
5.8	7.68	4.92	9.08	11.80	9.69
7.5	7.42	12.46	8.18	14.5	8.15
8.08	7.43	7.75	7.65	16.16	7.59

Table 8. Comparison with literature.

Ref	**Antenna size (mm^3) /Substrate**	**Reflector size (mm^3)-material/ type/array**	**Operating Bands (GHz)**	**Gain (dB)**	**FBR (dB)**	**Flexibility**	**SAR (W/Kg)**			**Polarization type**
							1 g	**d (mm)**	**P_{in} (W)**	
[15]	$(36 \times 18 \times 0.1)$ Ultralam 3550	$(86 \times 86 \times 1.52)$ -(RO 3003) 4×4-AMC	3.5 5.8	9.07 7.665	25	Yes	0.9 0.3	-	-	LP
[28]	$(34 \times 23 \times 1.6)$ FR4	$(45 \times 45 \times 2.1)$ -FR4/ 3×3-AMC	2.4 3.5 5.8	5.8 4.49 6.49	-	-	-			LP
[29]	$(80 \times 61 \times 1)$ Felt	$(100 \times 100 \times 2)$- Felt/ 5×5-AMC	4.55–13 UWB	6	> 15	Yes	0.1	-	-	LP
[16]	$(35 \times 27 \times 2.5)$ Felt	$(62 \times 62 \times 3)$- Felt/ 3×3-AMC	3.5 5.8	6.6 7.2	> 18	yes	0.12 0.04	3	0.1	CP
[31]	$(64 \times 64 \times 1.6)$ FR4	$(64 \times 64 \times 1.6)$- FR4 4×4-AMC	3.36 5.96 9.09	3.77 6.29 11.16	-	-	-	-	-	LP
[17]	$(40 \times 28 \times 3)$ PDMS	$(147 \times 147 \times 3)$- PDMS /$3 \times 3$-AMC	2.45 5.8	3.58 6.08	11.96 17.46	Yes	< 0.043	10	-	LP
[18]	$(70 \times 76 \times 3)$ Rogers-RO3003	$(130.8 \times 130.8 \times 3)$- Rogers (Ro 3003) 4×4-EBG	1.58 2.43	5.1 5.03	21.88 24.5	Semi flex	< 0.040	5	0.5	CP/LP
[20]	$(124 \times 90 \times 1)$ Jeans	$(150 \times 150 \times 1)$- Jeans/ 3×3-EBG	1.8 2.45	2.5 1.5	15.5 15.64	Yes	0.024, 0.01	1	-	LP
[21]	$(135 \times 135 \times 6)$ Polyester	$(135 \times 135 \times 6)$- Polyester 3×3-EBG	2.4	8.5	15.6	Yes	0.0698	10	1	LP
[32]	$(30 * 30 * 0.1)$ Polyimide	$(90 * 90 * 0.1)$- Polyimide/$3 * 3$-AMC	2.28–2.51 3.5–4 5.2–6	4.8 5.4 6.2	-	Yes	0.33	6	1	-
[22]	$(27.3 * 20 * 1.1)$ PDMS& Polyimide	$(60 * 50 * 1.1)$- PDMS & Polyimide/$6 * 5$ -EBG	4.5–6.5	11.8–13.6	-	Yes	0.59	4	-	-
Proposed	$(50 \times 30 \times 1)$ jeans	$(60 \times 60 \times 1)$- PDMS/ 3×3-AMC	3.5 5.8 7.5 8.08	7.53 9.08 8.18 7.65	10.72 11.80 14.5 16.16	Yes	< 0.504 < 1.016	3 3	0.5 1	CP/LP

3.3.1. Analysis of SAR with Input Power and d (mm) Variation

The proposed AMC integrated antenna holds high input power handling capability with satisfied SAR (1.6 W/kg) values which is required for high data rate wearable systems. The satisfying results are obtained with high input power variation (P_{in} = 1 W). Figure 27 illustrates the SAR distribution at 3.5, 5.8, 7.5, and 8.08 GHz frequencies for 1 g and 10 g of body tissues. High radiation absorption is observed at the antenna feed point only. The averaged SAR values of d and P_{in} variation are shown in Table 6.

In summary, the AMC reflector integrated antenna improves radiation performance in terms of gain and FBR as summarized in Table 7. The proposed antenna provides good isolation with the human body as well as low SAR with high input power to the antenna. The performance of the designed antenna is compared with existing literature in Table 8. The measured reflection coefficient of AMC antenna under human body loading and 60 mm radius cylindrical bend condition using Anritsu MS2037C VNA is presented in Figure 28.

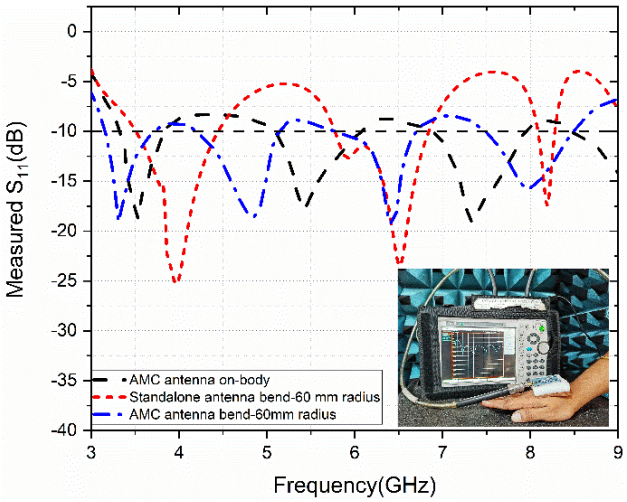

Figure 28. Measured S_{11} (dB) under human body loading and bend condition.

4. CONCLUSION

In this work, a flexible, low-profile AMC integrated quad-band textile antenna with radiation performance is proposed for WBAN applications. The antenna operates at 3.5, 5.8, 7.5, and 8.08 GHz frequencies with circular polarization at 3.5, 7.5, and 8.08 GHz. A good result is obtained in terms of gain and SAR at a separation of 10 mm from the human body surface. The observations show that the antenna suffers from frequency detuning, low FBR, and human body proximity effect. The demerits of the antenna were addressed by using AMC reflector which resonates at 3.5, 7.5, and 8.08 GHz. The proposed 3×3 AMC reflector provides a significant result in terms of improving gain, FBR, and low SAR ($<$ 0.504 W/kg for P_{in} = 0.5 W & $<$ 1.016 W/kg for P_{in} = 1 W) of high input power handling capability with high isolation over a low proximity distance of 3 mm. The analyzed results of the proposed AMC integrated antenna satisfy the requirements and challenges faced by the wearable antenna for body-centric communication applications.

ACKNOWLEDGMENT

Thankful to the AICTE-NDF/60483 and DST FIST-SR/FST/ET-II/2019/450.

REFERENCES

1. Hall, P. S. and Y. Hao, *Antennas and Propagation for Body-centric Wireless Communications*, 2nd Edition, Artech House, Inc., USA, 2012.
2. Mahfuz, M. M. H., et al., "Wearable textile patch antenna: Challenges and future directions," *IEEE Access*, Vol. 10, 38406–38427, 2022, doi: 10.1109/ACCESS.2022.3161564.
3. Shakib, M. N., M. Moghavvemi, and W. N. L. Binti Wan Mahadi, "Design of a tri-band off-body antenna for WBAN communication," *IEEE Antennas Wirel. Propag. Lett.*, Vol. 16, 210–213, 2017, doi: 10.1109/LAWP.2016.2569819.
4. El Gharbi, M., R. Fernández-García, S. Ahyoud, and I. Gil, "A review of flexible wearable antenna sensors: Design, fabrication methods, and applications," *Materials (Basel)*, Vol. 13, No. 17, 2020, doi: 10.3390/ma13173781.
5. Wang, J., et al., "Metantenna: When metasurface meets antenna again," *IEEE Trans. Antennas Propag.*, Vol. 68, No. 3, 1332–1347, 2020.
6. Zhang, K., P. J. Soh, and S. Yan, "Meta-wearable antennas — A review of metamaterial based antennas in wireless body area networks," *Materials (Basel)*, Vol. 14, No. 1, 149, 2021.
7. Dewan, R., et al., "Artificial magnetic conductor for various antenna applications: An overview," *Int. J. RF Microw. Comput. Eng.*, Vol. 27, No. 6, e21105, 2017.
8. Balanis, C. A., M. A. Amiri, A. Y. Modi, S. Pandi, and C. R. Birtcher, "Applications of AMC-based impedance surfaces," *EPJ Appl. Metamat.*, Vol. 5, 3, 2018, doi: 10.1051/epjam/2017010.
9. Zhang, K., G. A. E. Vandenbosch, and S. Yan, "A novel design approach for compact wearable antennas based on metasurfaces," *IEEE Trans. Biomed. Circuits Syst.*, Vol. 14, No. 4, 918–927, 2020, doi: 10.1109/TBCAS.2020.3010259.
10. Alemaryeen, A. and S. Noghanian, "Crumpling effects and specific absorption rates of flexible AMC integrated antennas," *IET Microwaves, Antennas & Propag.*, Vol. 12, No. 4, 627–635, 2018, doi: https://doi.org/10.1049/iet-map.2017.0652.
11. Hazarika, B., B. Basu, and A. Nandi, "An artificial magnetic conductor-backed monopole antenna to obtain high gain, conformability, and lower specific absorption rate for WBAN applications," *Int. J. RF Microw. Comput. Eng.*, Vol. 30, No. 12, e22441, 2020, doi: https://doi.org/10.1002/mmce.22441.
12. Arif, A., M. Zubair, M. Ali, M. U. Khan, and M. Q. Mehmood, "A compact, low-profile fractal antenna for wearable on-body WBAN applications," *IEEE Antennas Wirel. Propag. Lett.*, Vol. 18, No. 5, 981–985, 2019, doi: 10.1109/LAWP.2019.2906829.
13. Jiang, Z. H., D. E. Brocker, P. E. Sieber, and D. H. Werner, "A compact, low-profile metasurface-enabled antenna for wearable medical body-area network devices," *IEEE Trans. Antennas Propag.*, Vol. 62, No. 8, 4021–4030, 2014, doi: 10.1109/TAP.2014.2327650.
14. Kokolia, M. and Z. Raida, "Textile-integrated microwave components based on artificial magnetic conductor," *Int. J. Numer. Model. Electron. Networks, Devices Fields*, Vol. 34, No. 4, e2864, 2021, doi: https://doi.org/10.1002/jnm.2864.
15. El Atrash, M., M. A. Abdalla, and H. M. Elhennawy, "A wearable dual-band low profile high gain low SAR antenna AMC-backed for WBAN applications," *IEEE Trans. Antennas Propag.*, Vol. 67, No. 10, 6378–6388, 2019.
16. Yang, H., X. Liu, Y. Fan, and L. Xiong, "Dual-band textile antenna with dual circular polarizations using polarization rotation AMC for off-body communications," *IEEE Trans. Antennas Propag.*, 1, 2022, doi: 10.1109/TAP.2021.3138504.
17. Ramli, M. N., P. J. Soh, M. F. Jamlos, H. Lago, N. M. Aziz, and A. A. Al-Hadi, "Dual-band wearable fluidic antenna with metasurface embedded in a PDMS substrate," *Appl. Phys. A*, Vol. 123, No. 2, 149, 2017.
18. Paracha, K. N., et al., "A low profile, dual-band, dual polarized antenna for indoor/outdoor wearable application," *IEEE Access*, Vol. 7, 33277–33288, 2019.

19. Dey, A. B., D. Mitra, and W. Arif, "Design of CPW fed multiband antenna for wearable wireless body area network applications," *Int. J. RF Microw. Comput. Eng.*, Oct. 2020, doi: 10.1002/mmce.22459.
20. Velan, S., et al., "Dual-band EBG integrated monopole antenna deploying fractal geometry for wearable applications," *IEEE Antennas Wirel. Propag. Lett.*, Vol. 14, 249–252, 2015, doi: 10.1109/LAWP.2014.2360710.
21. Abirami, B. S. and E. F. Sundarsingh, "EBG-backed flexible printed Yagi-Uda antenna for on-body communication," *IEEE Trans. Antennas Propag.*, Vol. 65, No. 7, 3762–3765, 2017, doi: 10.1109/TAP.2017.2705224.
22. Zu, H., B. Wu, P. Yang, W. Li, and J. Liu, "Wideband and high-gain wearable antenna array with specific absorption rate suppression," *Electronics*, Vol. 10, No. 17, 2021, doi: 10.3390/electronics10172056.
23. Cheng, Y.-F., X. Ding, B.-Z. Wang, and W. Shao, "An azimuth-pattern-reconfigurable antenna with enhanced gain and front-to-back ratio," *IEEE Antennas Wirel. Propag. Lett.*, Vol. 16, 2303–2306, 2017, doi: 10.1109/LAWP.2017.2715373.
24. Sarkar, P. P., "Compact ultra-wideband antenna: Improvement of gain and FBR across the entire bandwidth using FSS," *IET Microwaves, Antennas Propag.*, Vol. 14, No. 1, 66–74(8), Jan. 2020. [Online]. Available: https://digital-library.theiet.org/content/journals/10.1049/iet-map.2019.0536.
25. Kumar, C. and D. Guha, "Mitigating backside radiation issues of defected ground structure integrated microstrip patches," *IEEE Antennas Wirel. Propag. Lett.*, Vol. 19, No. 12, 2502–2506, 2020, doi: 10.1109/LAWP.2020.3037219.
26. Xu, Y., N.-W. Liu, and L. Zhu, "Proposal and design of an end-fire slot antenna with low back-lobe and improved front-to-back ratio," *Int. J. RF Microw. Comput. Eng.*, Vol. 31, No. 2, e22508, 2021, doi: https://doi.org/10.1002/mmce.22508.
27. Alam, M., M. Siddique, B. K. Kanaujia, M. T. Beg, S. Kumar, and K. Rambabu, "Meta-surface enabled hepta-band compact antenna for wearable applications," *IET Microwaves, Antennas & Propag.*, Vol. 13, No. 13, 2372–2379, 2019, doi: https://doi.org/10.1049/iet-map.2018.6212.
28. Yu, C., S. Yang, Y. Chen, and D. Zeng, "Radiation enhancement for a triband microstrip antenna using an AMC reflector characterized with three zero-phases in reflection coefficient," *Journal of Electromagnetic Waves and Applications*, Vol. 33, No. 14, 1846–1859, 2019, doi: 10.1080/09205071.2019.1645743.
29. Yalduz, H., T. E. Tabaru, V. T. Kilic, and M. Turkmen, "Design and analysis of low profile and low SAR full-textile UWB wearable antenna with metamaterial for WBAN applications," *AEU — Int. J. Electron. Commun.*, Vol. 126, 153465, 2020, doi: https://doi.org/10.1016/j.aeue.2020.153465.
30. Gong, Y., S. Yang, B. Li, Y. Chen, F. Tong, and C. Yu, "Multi-band and high gain antenna using AMC ground characterized with four zero-phases of reflection coefficient," *IEEE Access*, Vol. 8, 171457–171468, 2020.
31. Ghosh, A., V. Kumar, G. Sen, and S. Das, "Gain enhancement of triple-band patch antenna by using triple-band artificial magnetic conductor," *IET Microwaves, Antennas Propag.*, Vol. 12, No. 8, 1400–1406, 2018.
32. Lai, J., J. Wang, W. Sun, R. Zhao, and H. Zeng, "A low profile artificial magnetic conductor based tri-band antenna for wearable applications," *Microw. Opt. Technol. Lett.*, Vol. 64, No. 1, 123–129, 2022, doi: https://doi.org/10.1002/mop.33040.
33. "Shielding and conductive fabrics," Less EMF, 2015.
34. Fields, R. E., "Evaluating compliance with FCC guidelines for human exposure to radiofrequency electromagnetic fields," *OET Bull.*, Vol. 65, No. 10, 1997.
35. Sharma, P. K., N. Gupta, and P. I. Dankov, "Characterization of polydimethylsiloxane (PDMS) as a wearable antenna substrate using resonance and planar structure methods," *AEU — Int. J. Electron. Commun.*, Vol. 127, 153455, 2020, doi: https://doi.org/10.1016/j.aeue.2020.153455.
36. Langley, R. J. and E. A. Parker, "Double-square frequency-selective surfaces and their equivalent circuit," *Electron. Lett.*, Vol. 19, No. 17, 675–677, 1983.